Article:
Lim, YL, Taimre, T, Bertling, K et al. (12 more authors) (2014) High-contrast coherent terahertz imaging of porcine tissue via swept-frequency feedback interferometry. Biomedical Optics Express, 5 (11). 11. pp. 3981-3989. ISSN 2156-7085

https://doi.org/10.1364/BOE.5.003981

High-contrast coherent terahertz imaging of porcine tissue via swept-frequency feedback interferometry

Yah Leng Lim,[1] Thomas Taimre,[2] Karl Bertling,[1] Paul Dean,[3] Dragan Indjin,[3] Alexander Valavanis,[3] Suraj P. Khanna,[3] Mohammad Lachab,[3] Helmut Schaider,[4] Tarl W. Prow,[4] H. Peter Soyer,[4] Stephen J. Wilson,[1] Edmund H. Linfield,[3] A. Giles Davies,[3] and Aleksandar D. Rakić[1,*]

[1]*School of Information Technology and Electrical Engineering, The University of Queensland, Brisbane, QLD 4072, Australia*

[2]*School of Mathematics and Physics, The University of Queensland, Brisbane, QLD 4072, Australia*

[3]*School of Electronic and Electrical Engineering, University of Leeds, Leeds LS2 9JT, United Kingdom*

[4]*Dermatology Research Centre, The University of Queensland, School of Medicine, Translational Research Institute, Brisbane, QLD 4102, Australia*

[*]*rakic@itee.uq.edu.au*

Abstract: There is considerable interest in the interrogation of biological tissue at terahertz (THz) frequencies, largely due to the contrast in the optical properties of different biological tissues which occur in this electro-magnetic radiation band. Of particular interest are THz biomedical images, which have the potential to highlight different information than those acquired in other frequency bands, thereby providing an augmented picture of biological structures. In this work, we demonstrate the feasibility of an interferometric biological imaging technique using a THz quantum cascade laser (QCL) operating at 2.59 THz to perform coherent imaging of porcine tissue samples.

OCIS codes: (170.6795) Terahertz imaging; (120.3180) Interferometry; (140.5965) Semiconductor lasers, quantum cascade.

References and links

1. B. B. Hu and M. C. Nuss, "Imaging with terahertz waves," Opt. Lett. **20**, 1716–1718 (1995).
2. S. Smye, J. Chamberlain, A. Fitzgerald, and E. Berry, "The interaction between terahertz radiation and biological tissue," Phys. Med. Biol. **46**, R101 (2001).
3. A. Fitzgerald, E. Berry, N. Zinov'ev, S. Homer-Vanniasinkam, R. Miles, J. Chamberlain, and M. Smith, "Catalogue of human tissue optical properties at terahertz frequencies," J. Biol. Phys. **29**, 123–128 (2003).
4. S. Huang, Y. Wang, D. Yeung, A. Ahuja, Y. Zhang, and E. Pickwell-MacPherson, "Tissue characterization using terahertz pulsed imaging in reflection geometry," Phys. Med. Biol. **54**, 149 (2009).
5. R. M. Woodward, B. E. Cole, V. P. Wallace, R. J. Pye, D. D. Arnone, E. H. Linfield, and M. Pepper, "Terahertz pulse imaging in reflection geometry of human skin cancer and skin tissue," Phys. Med. Biol. **47**, 3853 (2002).
6. V. P. Wallace, A. J. Fitzgerald, E. Pickwell, R. J. Pye, P. F. Taday, N. Flanagan, and T. Ha, "Terahertz pulsed spectroscopy of human basal cell carcinoma," Appl. Spectrosc. **60**, 1127–1133 (2006).

7. C. Yu, S. Fan, Y. Sun, and E. Pickwell-MacPherson, "The potential of terahertz imaging for cancer diagnosis: A review of investigations to date," Quant. Imaging Med. Surg. **2**, 33–45 (2012).
8. C. S. Joseph, R. Patel, V. A. Neel, R. H. Giles, and A. N. Yaroslavsky, "Imaging of ex vivo nonmelanoma skin cancers in the optical and terahertz spectral regions optical and terahertz skin cancers imaging," J. Biophotonics **7**, 295–303 (2012).
9. J. Xu, K. W. Plaxco, and S. J. Allen, "Absorption spectra of liquid water and aqueous buffers between 0.3 and 3.72 THz," J. Chem. Phys **124**, 36101–36101 (2006).
10. E. Pickwell, B. Cole, A. Fitzgerald, M. Pepper, and V. Wallace, "In vivo study of human skin using pulsed terahertz radiation," Phys. Med. Biol. **49**, 1595 (2004).
11. E. Pickwell and V. Wallace, "Biomedical applications of terahertz technology," J. Phys. D: Appl. Phys. **39**, R301 (2006).
12. M. Naftaly, "Metrology issues and solutions in THz time-domain spectroscopy: Noise, errors, calibration," IEEE Sens. J. **13**, 8 –17 (2013).
13. R. Köhler, A. Tredicucci, F. Beltram, H. E. Beere, E. H. Linfield, A. G. Davies, D. A. Ritchie, R. C. Iotti, and F. Rossi, "Terahertz semiconductor-heterostructure laser," Nature **417**, 156–159 (2002).
14. L. Li, L. Chen, J. Zhu, J. Freeman, P. Dean, A. Valavanis, A. Davies, and E. Linfield, "Terahertz quantum cascade lasers with >1 W output powers," Electron. Lett. **50**, 309–311 (2014).
15. J. Darmo, V. Tamosiunas, G. Fasching, J. Kröll, K. Unterrainer, M. Beck, M. Giovannini, J. Faist, C. Kremser, and P. Debbage, "Imaging with a terahertz quantum cascade laser," Opt. Express **12**, 1879–1884 (2004).
16. S. M. Kim, F. Hatami, J. S. Harris, A. W. Kurian, J. Ford, D. King, G. Scalari, M. Giovannini, N. Hoyler, J. Faist, and G. Harris, "Biomedical terahertz imaging with a quantum cascade laser," Appl. Phys. Lett. **88**, 153903 (2006).
17. A. D. Rakić, T. Taimre, K. Bertling, Y. L. Lim, P. Dean, D. Indjin, Z. Ikonić, P. Harrison, A. Valavanis, S. P. Khanna, M. Lachab, S. J. Wilson, E. H. Linfield, and A. G. Davies, "Swept-frequency feedback interferometry using terahertz frequency QCLs: a method for imaging and materials analysis," Opt. Express **21**, 22194–22205 (2013).
18. Z. Taylor, R. Singh, M. Culjat, J. Suen, W. Grundfest, H. Lee, and E. Brown, "Reflective terahertz imaging of porcine skin burns," Opt. Lett. **33**, 1258–1260 (2008).
19. A. Dobroiu, M. Yamashita, Y. N. Ohshima, Y. Morita, C. Otani, and K. Kawase, "Terahertz imaging system based on a backward-wave oscillator," Applied optics **43**, 5637–5646 (2004).
20. Y. Sun, B. M. Fischer, and E. Pickwell-MacPherson, "Effects of formalin fixing on the terahertz properties of biological tissues," J. Biomed. Opt. **14**, 064017–064017 (2009).
21. M. He, A. K. Azad, S. Ye, and W. Zhang, "Far-infrared signature of animal tissues characterized by terahertz time-domain spectroscopy," Opt. Commun. **259**, 389–392 (2006).
22. S. J. Oh, S.-H. Kim, K. Jeong, Y. Park, Y.-M. Huh, J.-H. Son, and J.-S. Suh, "Measurement depth enhancement in terahertz imaging of biological tissues," Opt. Express **21**, 21299–21305 (2013).
23. P. Dean, Y. L. Lim, A. Valavanis, R. Kliese, M. Nikolić, S. P. Khanna, M. Lachab, D. Indjin, Z. Ikonić, P. Harrison, A. D. Rakić, E. H. Linfield, and A. G. Davies, "Terahertz imaging through self-mixing in a quantum cascade laser," Opt. Lett. **36**, 2587–2589 (2011).
24. S. Donati, "Responsivity and noise of self-mixing photodetection schemes," IEEE J. Quantum Electron. **47**, 1428–1433 (2011).
25. D. B. Bennett, W. Li, Z. D. Taylor, W. S. Grundfest, and E. R. Brown, "Stratified media model for terahertz reflectometry of the skin," IEEE Sensors J. **11**, 1253 – 1262 (2011).

1. Introduction

Characterisation of biological materials in the terahertz (THz) frequency range has attracted considerable interest, largely due to the contrast in the optical properties of different biological tissues that is known to exist in this electro-magnetic radiation band [1–4]. These differing THz properties offer a new means of understanding the structure and function of specialised tissue, as well as the potential for discriminating normal from pathological material [5–7]. Of particular interest are THz biomedical images, which have the potential to highlight different information than those acquired at other frequencies, thereby providing an augmented picture of biological structures [8]. One important class of these THz images are functional images of relative water saturation, made possible due to the strong absorption of THz radiation by liquid water [9]. Consequently, skin, particularly *in vivo*, is one target tissue of interest for these imaging techniques, since this strong attentuation of THz radiation by water effectively ensures little or no reflected radiation from tissue structures deeper than the dermis. The possibility of

discriminating between tissue types and pathology in superficial skin has wide-ranging clinical implications although clinical up-take is ultimately limited by the complexity and cost of the interrogation system used.

Imaging of biological tissues at THz frequencies has conventionally been undertaken using THz pulsed imaging (TPI) [4–7, 10, 11]. These systems are inherently broadband, and are typically effective up to ∼2 THz [12]. Simplifications of the sensing system with improvements in signal-to-noise ratio (SNR) are desirable, particularly above ∼2 THz, as is a compact, robust architecture. Recently, quantum cascade lasers (QCLs) have emerged as the stable, high-power source of choice in the laboratory for radiation between ∼1 to 5 THz [13], with output powers greater than 1 Watt having been demonstrated in pulsed operation [14]. Incoherent imaging of biological tissues using QCLs has previously been demonstrated [15, 16]. However, these demonstrations used a transmission geometry (or double-pass transmission in the case of [15]), which is not applicable to *in vivo* studies.

In [17], we introduced a novel imaging and materials analysis scheme in the THz band that exploits the interferometric nature of optical feedback in a THz QCL to employ it as a homodyning transceiver. This results in a highly sensitive and compact scheme capable of probing coherently the radiation reflected from remote targets.In this paper, we apply our scheme to the reflection-mode imaging of excised porcine tissue (commonly used as an animal model for human tissue [18–20]), and produce high-contrast THz images through two different reductions of the information-rich interferometric signals — one containing predominantly amplitude information and the other predominantly containing phase information. In these images, clear contrast between different tissue types is observed (as is expected from previous THz characterisation of tissue [3, 20, 21]), corresponding to differing interferometric signal morphology. Additionally, there are distinct features observable in the *en face* images that are not apparent in the visible. Moreover, when different tissue types are plotted in amplitude–phase space, they form distinct clusters. This clustering of tissue signatures hints at the possibility for classification of skin tissue types based on their interferometric THz signals. Through experiment, we establish that the practically useful penetration depth of our QCL beam is over 100 μm in the reflection mode, which is consistent with other THz frequency techniques [22]. This work represents the first demonstration of coherent imaging of biological materials using a THz QCL source and points the way to non-invasive *in vivo* imaging in the THz.

2. Experimental Setup

Figure 1 shows the schematic diagram of the experimental setup. The THz QCL (operating at 2.59 THz) consisted of a 11.6 μm-thick GaAs/AlGaAs bound-to-continuum active-region that was processed into a semi-insulating surface-plasmon ridge waveguide with dimensions 1.78 mm × 140 μm. The QCL was mounted onto the cold finger of a continuous-flow cryostat fitted with a polyethylene window and operated at a heat sink temperature of 15 K. Radiation from the QCL was collimated using a 2 inch (50.8 mm) diameter off-axis parabolic reflector with a 4 inch (101.6 mm) focal length and focussed at normal incidence onto the target using a second identical mirror, resulting in an approximately circular beam spot at the focus with ∼200 μm $1/e^2$ diameter. The total optical path between the THz QCL source and target was 568.2 mm through an ambient (unpurged) atmosphere.

The laser was driven by a current source at $I_{dc} = 0.43$ A, slightly above the threshold ($I_{th} = 0.4$ A), where the sensitivity to optical feedback is at a maximum [23, 24]. A 1 kHz modulating saw-tooth current signal (50 mA peak-to-peak amplitude) was superimposed on the dc current resulting in a linear frequency sweep of 600 MHz. Owing to optical feedback from the material under test, the self-mixing waveform containing information about the target is embedded in the voltage signal measured across the terminals of the QCL. This voltage was amplified by

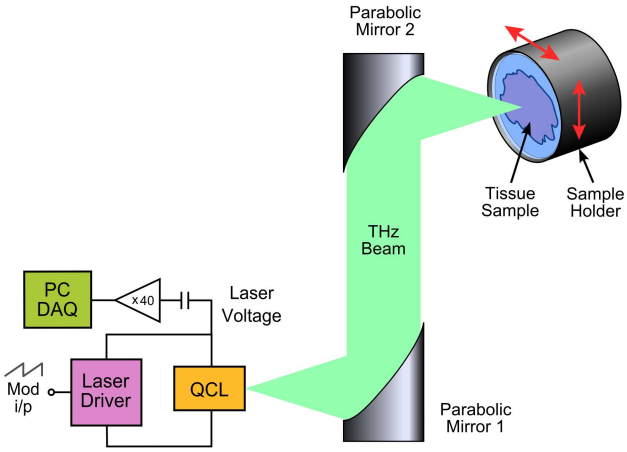

Fig. 1. Schematic diagram of the setup used for tissue samples measurements. The operating principles of the setup have been discussed in detail previously [17].

a differential amplifier with 40 times gain and subsequently measured using a 16-bit data PC-based data-acquisition (DAQ) card.

For image acquisition, targets were raster-scanned in two dimensions using a two-axis computer-controlled translation stage. The time domain traces were acquired at each node of a 101×101 square grid with spatial resolution of 200 µm (standard resolution), or on a 51×301 rectangular grid with spatial resolution of 50 µm (high resolution). As such, images acquired in the focal plane at standard resolution have minimal overlap of illuminated portions of the target between adjacent pixels, whereas high resolution images experience analogue smoothing due to non-negligible overlap. At each spatial pixel of the target, the voltage signal was recorded as the average of 128 time-domain traces. Therefore the complete set of experimental data contains 101×101 (or 51×301) time-domain waveforms, each corresponding to one spatial pixel on the target.

2.1. Sample Preparation

Two sets of experiments were performed using the common experimental setup, differing only in sample preparation and purpose. For the first set of experiments, designed to examine THz imaging of biological tissue with our scheme, two pieces of fresh tissue from the abdomen of a pig were placed in an internally threaded aluminium tube with a 1 inch (25.4 mm) internal diameter, pre-mounted with an adjustable acrylic backing plate [see Fig. 2(a)]. A polymethylpentene (TPX) window 1 inch (25.4 mm) in diameter and ≈ 2 mm thick was placed in front of the tissue samples. A retaining ring was used to affix the tissue between the window and the backing, ensuring no air-gaps remained. The target was aligned perpendicular to the optical axis, and a triangular piece of aluminium film inserted between the TPX window and the tissue sample was used to aid positioning of the surface of the tissue sample at the THz beam focus.

One piece of tissue was placed with its cross-section facing the TPX window [above aluminium separator in Fig. 2(a)]. From the top of this tissue cross-section down to the aluminium separator, the layers of tissue are muscle, fat, and skin. The second piece of tissue was placed *en face* [below aluminium separator in Fig. 2(a)], so that only the surface of the skin was facing the TPX window. Both tissue samples were in excess of 5 mm thick, to effectively ensure no

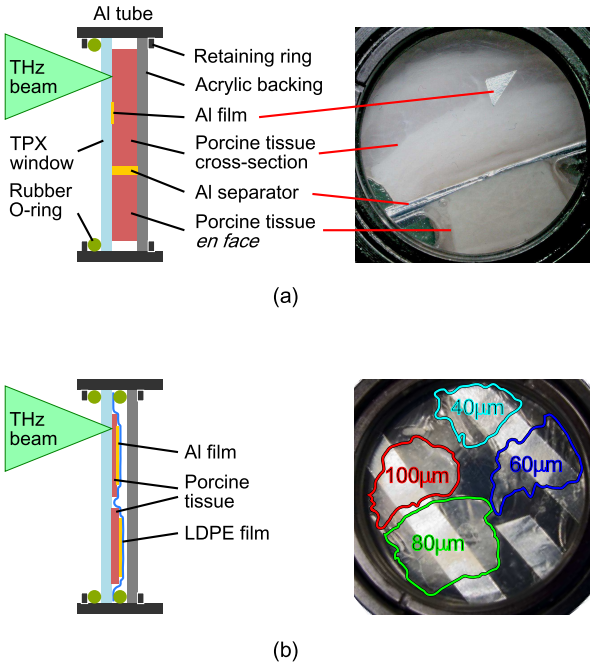

Fig. 2. Visual images and descriptions of the mounted porcines tissue samples. (a) shows two pieces of fresh tissue from the abdomen of a pig placed in an internally threaded aluminium tube. The tissue sample above the aluminium separator was placed with its cross-section facing the TPX window; the tissue sample below the aluminium separator was placed *en face* with its skin surface facing the TPX window. (b) shows the thin slices of fresh porcine abdominal skin of different thicknesses (40 μm – 100 μm) placed behind the TPX window.

THz reflection from the backing plate [25].

For the second set of experiments, designed to examine the penetration depth in tissue detectable by our scheme, four thin pieces of fresh porcine abdominal skin, were microtomed to thicknesses of 40, 60, 80, and 100 μm respectively. Each piece was carefully placed onto the TPX window. To characterise the penetration depth of the thin tissue samples, three strips of aluminium film were positioned on the rear surface of these samples, ensuring partial overlap with all four pieces of tissue. A layer of low-density polyethylene (LDPE) film was then placed over the aluminium-backed pieces of tissue, kept in place by an o-ring, which itself was secured by a backing plate [see Fig. 2(b)]. This ensured that the samples retained their moisture whilst being maintained in position. The target was aligned perpendicular to the optical axis, and a strip of aluminium film mounted just behind TPX window, without obscuring the tissue, was again used to ensure that the THz beam was focussed to that imaging plane.

3. Results and Discussion

For both experiments, a two-dimensional array of time-domain waveforms was acquired, with one waveform associated with each pixel in the array. Experimentally-acquired signals were treated as described in [17]. The resulting interferometric waveforms are information rich, with morphological features such as signal amplitude, peak shape, and peak position containing information about the target. As such, there is no single way to reduce this array of wave-

forms into an array of numbers (thereby forming an image). For the two sets of experiments performed herein, we adopted two such waveform reductions corresponding to the most prominent characteristics of this self-mixing signal — its amplitude and relative peak position, which are closely related to the target reflectivity and the phase-shift on reflection. The first reduction is a trimmed-mean of the self-mixing signal — a measure of average signal strength with an equal proportion of high and low extremes excluded from the ensemble, and therefore containing predominantly amplitude information. The second is the temporal position of the peak in the self-mixing signal — a measure of the relative position of the interferometric peaks within the waveform, and therefore containing predominantly phase information.

Figures 3(a) and (b) show these two THz images. Contrast between the different tissue types (from top to bottom: muscle; sub-dermal fat; and skin) in the cross-section part of the target (i.e. above the aluminium separator) is clearly visible in the amplitude-like image [Fig. 3(a)], as expected from [20,21]. Moreover, in the *en face* part of the target (i.e. below the aluminium separator), clear features are present in both the amplitude-like and the phase-like images [Figs. 3(a) and (b), respectively] that are not evident in the visible image, as can be seen by comparison with the photograph shown in Fig. 2(a)]. Figures 3(c)–(h) depict heat maps of exemplar self-mixing signals obtained from a high resolution scan of a vertical strip of the same target [region shown in the inset to Fig. 3(a); different markers correspond to different tissue types, and indicate the location from which these exemplar signals were taken]. It is clear from Figs. 3(c)–(h) that each waveform differs in one or more morphological aspects, not the least of which are the amplitude and/or phase. Examining each signature in turn from the skin surface, a characteristic signal morphology is observed for: c) epidermis; d) dermis; e) sub-dermal fascia and connective tissue; g) fat; and h) muscle. Figure 3(i) plots the amplitude–phase reductions of the exemplar self-mixing signals from Fig. 3(c)–(h), with each tissue type retaining its marker. Note that different tissue types appear to form clusters in amplitude–phase space, suggesting future potential for discriminating between tissue types based on the information contained in the self-mixing signals.

As one would expect, self-mixing signals from the aluminium separator exhibit the highest level of feedback, as is indicated by the "sharp" peaks present in the waveforms. Moreover, the heat map representation suggests that there are a number of distinct phase-shifts on reflection present; this can be explained as a consequence of the wrinkled surface of the rolled section of aluminium film which forms the aluminium separator.

The features observed in the two THz images in Fig. 3(a) and (b) have also been correlated with those observed by hematoxylin and eosin (H&E) stained visible microscopy of the same specimen after THz examination. Figure 4(a) shows the visual image of the sample, the lower part of the figure within the blue rectangular frame being the *en face* skin sample. Figure 4(c) shows the corresponding (amplitude-like) THz image of the same area. As can be seen, the visual image shows no observable structure within the selected area, while four features are distinctly observable in the THz image. To clarify the nature of these features, we have microtomed the sample, removing the top layer of the skin to the depth of approximately 60 μm, the resulting plane having no more the 5 degrees inclination with respect to the original surface of the skin. This *en face* surface is shown in the H&E stained microscopic image in Fig. 4(b), allowing for the identification of the features observed in the THz image as: blood vessels (i & iv), arteriole and venule pair (iii), and sebaceous gland (ii). Geometric distortion due to the fixation and the sectioning process prevents us from seeing these structures as directly overlaying their THz image equivalents.

Figure 5(a) and (b) shows the amplitude-like and phase-like THz images, respectively, obtained from our second set of experiments designed to determine the detectable penetration depth within the samples. By comparison with the visible image shown in Fig. 2(b), it can be

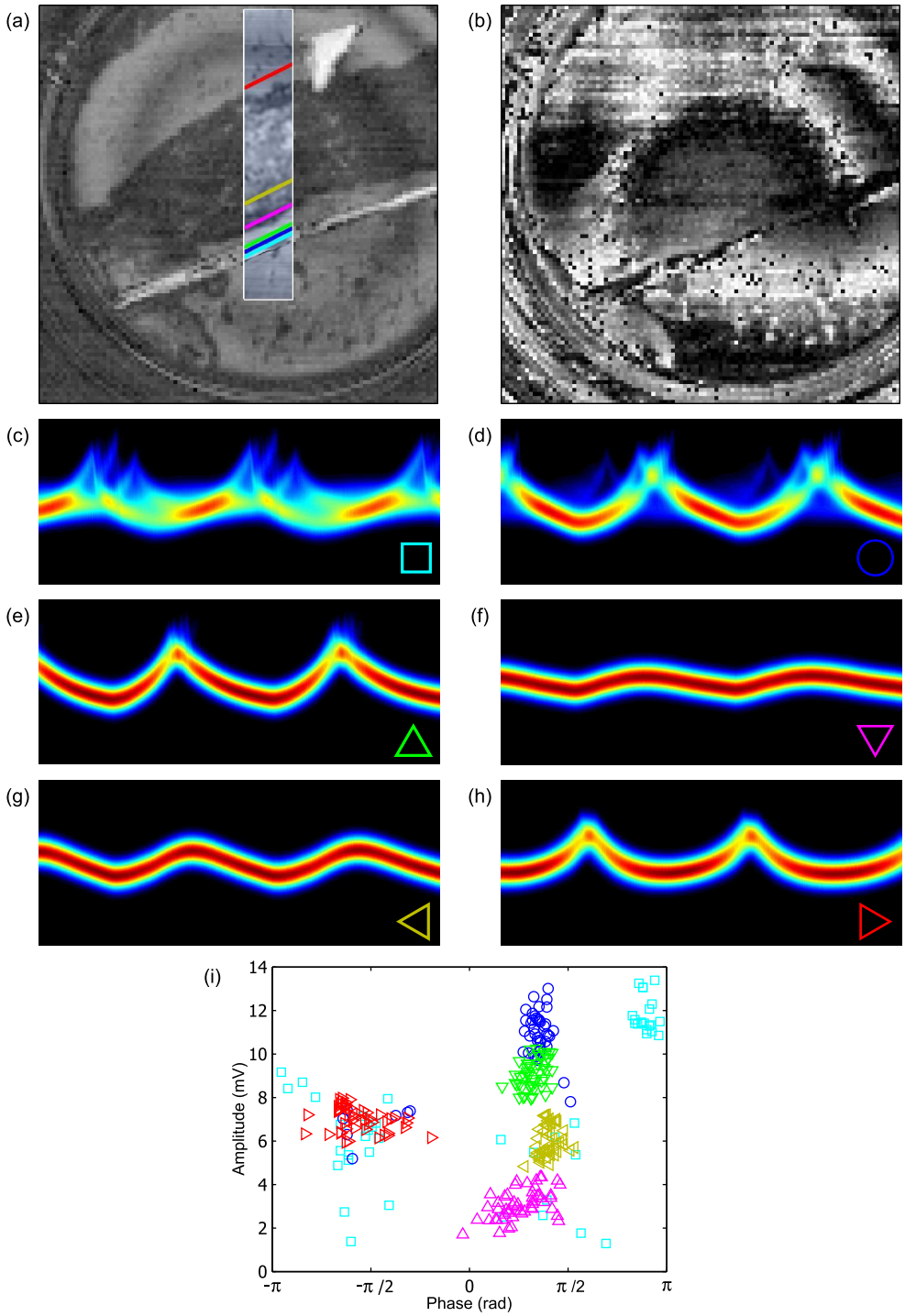

Fig. 3. THz porcine tissue imaging using self-mixing interferometry [the sample was described in Fig. 2(a)]. (a) is the amplitude-like imaging modality based on a 101 $\times$ 101 array of self-mixing waveforms [Inset: high resolution image based on a 51 $\times$ 301 array], (b) is the phase-like imaging modality, (c)–(h) is the heat map of self-mixing waveforms for different tissue types associated with the color markers overlayed in (a). Specifically the tissue types are: (c) Aluminium separator; (d) Epidermis; (e) Upper dermis; (f) Lower dermis; (g) Sub-dermal fat; (h) muscle tissue; (i) presents the corresponding amplitude-phase plots of waveforms (c)–(h). The mark of each tissue type appear to form natural clusters.

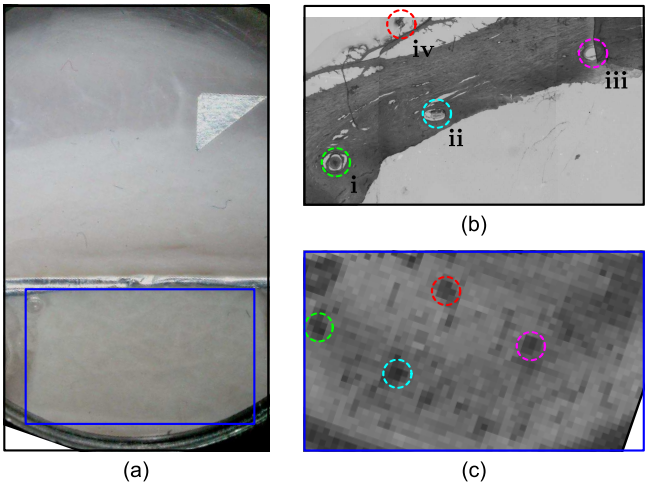

Fig. 4. (a) shows the visual image of the sample. The comparison area is highlighted (blue rectangle). (b) Showing H&E *en face* section visible microscopic view of the sample tissue in Fig. 3. Blood vessels (i & iv), arteriole and venule pair (iii), and sebaceous gland (ii) correspond to distinct features seen in (c) the amplitude-like THz derived image.

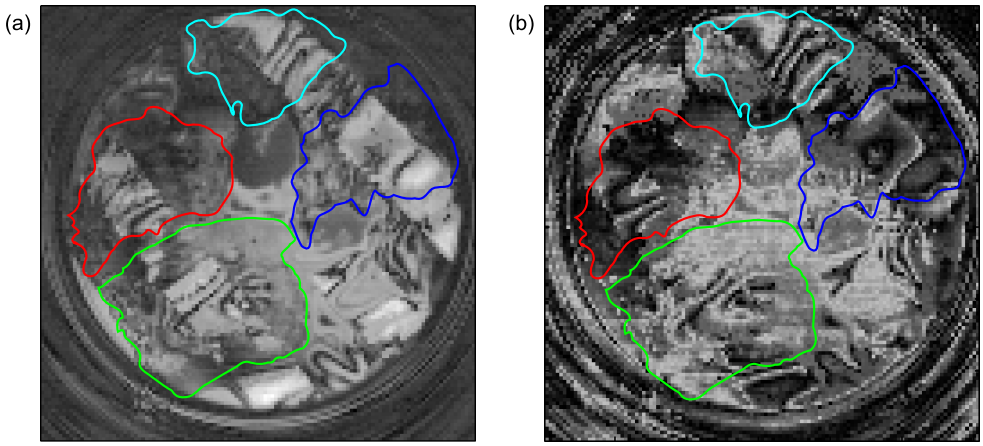

Fig. 5. THz images for porcine tissue depth penetration experiments using self-mixing interferometry [the sample was described in Fig. 2(b)]. (a) is the amplitude like imaging modality, (b) is the phase like imaging modality.

seen that contrast between aluminium-backed skin and non-backed skin is clearly visible in all four pieces of skin and in both THz images. This demonstrates experimentally that our scheme is able to obtain signal from at least 100 μm deep in skin tissue in the reflection mode.

4. Conclusion

In this work, we demonstrated the feasibility of an interferometric biological imaging technique using a THz QCL operating at 2.59 THz with porcine tissue samples. We produced coherent THz images showing the scheme's capability to discriminate between different tissue types,

namely muscle, sub-dermal fat, and skin. This is further supported by the clustering of signals observed for different these tissue types, with the inclusion of the epidermis, upper dermis and lower dermis. Moreover, features observed in THz images of an *en face* tissue sample, but not apparent in the optical image, were found to be correlated with sub-surface structures revealed in a histological stain. The resolution and penetration depth of this scheme were found to be suitable for detection of sub-surface features of skin tissues, to a penetration depth exceeding 100 μm.

Acknowledgments

This research was supported under Australian Research Council's Discovery Projects funding scheme (DP 120 103703) and a Cancer Research UK Leeds Centre Development Fund Equipment award (Grant number C37059/A16369). We also acknowledge support of the ERC 'NOTES' and 'TOSCA' programmes, the Royal Society, the Wolfson Foundation, and the European Cooperation in Science and Technology (COST) Action BM1205. Y.L.L. acknowledges support under the Queensland Government's Smart Futures Fellowships programme. P.D. acknowledges support from the EPSRC (UK).